Proceedings of the 2005 IEEE
International Conference on Robotics and Automation
Barcelona, Spain, April 2005

Shape, Motion, and Parameter Estimation of Large Flexible Space Structures using Range Images

Matthew D. Lichter and Steven Dubowsky
Department of Mechanical Engineering
Massachusetts Institute of Technology
Cambridge, MA, USA
{ lichter | dubowsky } @mit.edu

Abstract – Future space missions are expected to use robotic systems to assemble, inspect, and maintain large space structures in orbit. To carry out these tasks, robots need to know the deformations and motions of the structures with which they interact. This paper presents a method for efficiently estimating the shape, motion, and dynamic model parameters of a vibrating space structure using range imaging sensors. The method assumes that the mode shapes are approximately known a priori. A Kalman filter exploits a mechanics-based dynamic model to extract the modal frequencies and damping as well as the modal coefficients and their time rate of change. This paper presents theoretical development as well as simulation and experimental results. Results on computational efficiency are included.

Index Terms – space structures, range images, shape estimation, motion estimation, cooperative sensing.

I. Introduction

Future space missions are expected to use autonomous robotic systems to assemble, inspect, and maintain large space structures in orbit [1][2][3]. Such structures include the International Space Station, large synthetic aperture telescopes, and space solar power systems [4][5]. To safely plan and control tasks, robotic systems require knowledge of structural deformations and motions. Remote sensing and estimation of target dynamics and model parameters is expected to be a fundamental challenge for these missions.

Many researchers have examined the use of embedded sensors such as strain gauges and accelerometers to directly measure the motions and deformations of flexible structures [6][7][8]. However, the hardware costs and the complexity of this approach may be prohibitive for very large space structures that span hundreds or thousands of meters [9].

A potentially simpler approach would be to use the range imaging sensors that may be available from the free-flying robotic workers (see Fig. 1). Such sensors might include stereo cameras [10] and laser rangefinders [11]. However, there are a number of challenges to this approach. Range images can be highly noisy and data may be missing from many areas of the structure due to the harsh lighting conditions found in space. Strong sunlight, high-contrast scenes, and reflective materials (e.g. solar panels and metallic foils found on spacecraft) pose significant challenges to many image processing algorithms [12]. Tracking specific points on the structure can be very difficult as the lighting or sensor positions change. Complicating the problem is the fact that computational resources tend to be very limited in space-qualified hardware.

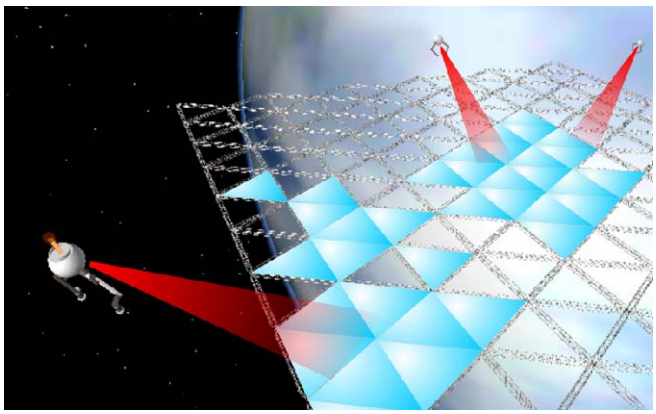

Fig. 1. Using onboard vision sensors to estimate structural information.

This paper presents a method for estimating the shape and motion of a region of interest on a flexible space structure, using data gathered from one or more 3-D range imaging sensors. This method takes advantage of a key feature of the application, which is that the dynamics of systems in space are very deterministic and can be modeled accurately. This allows a method that does *not* require the tracking of structural features over time. Further, it yields an estimator that is computationally efficient while being robust to substantial sensor noise and a priori uncertainty.

II. General Method

A. Assumptions

Sensors are assumed to provide discrete 3-D range image clouds of the structure at regular intervals. All points in the cloud are assumed to be captured at approximately the same instant in time. The time delay between the first and last data point captured is assumed to be small compared to the period of the highest natural frequency estimated. Sensor noise is assumed to be additive, white, and unbiased, but not necessarily Gaussian. If multiple cooperative sensors are used to gather range images, it is assumed that their relative poses are accurately known so that their data can be expressed in a common reference frame. Communication delays between sensors are assumed to be negligible.

This work is sponsored by the Japan Aerospace Exploration Agency (JAXA).

The structural dynamics are assumed to be linear or weakly nonlinear. The structure's mode shapes are assumed to be well-known to the estimator a priori. These could be provided using techniques such as finite element analysis and could be computed offline beforehand. Modal knowledge is assumed to be updated whenever the fundamental mode shapes change (e.g. due to a structural configuration change, added mass, etc.). A priori uncertainty in the modal frequencies is assumed to be bounded, on the order of ±20 percent of the true frequencies.

B. Approach

Let the natural mode shapes of the structure be denoted as $\Phi_i(x)$ for each mode i. For a linear elastic system, the dynamic response $z(x,t)$ of the structural deformations can be written as

$$z(x,t) = \sum_{i=1}^{m} A_i(t)\Phi_i(x) = A(t)^T \Phi(x) \qquad (1)$$

where $z(x,t)$ is the deflection from the structure's equilibrium state, m is the number of modes excited in the response, and $A_i(t)$ is the i^{th} modal coefficient, which oscillates sinusoidally with the i^{th} modal frequency ω_i. If modal damping exists, these sinusoids decay exponentially with rate α_i.

The goal is to estimate the time domain functions $A_i(t)$ for all modes of interest. This will reduce shape estimation to simply a modal reconstruction using the estimates of $A_i(t)$ and the mode shapes $\Phi_i(x)$.

Estimation of $A_i(t)$ will occur in two steps. First, modal decomposition in the spatial domain will be performed on the range image to arrive at a coarse estimate $\breve{A}_i(t)$. This estimate will then be filtered in the time domain using a Kalman filter to arrive at a refined estimate $\hat{A}_i(t)$. Note the hat notation used to denote coarse and refined estimates.

III. Modal Decomposition

The first step in the estimation process involves a modal decomposition of the visual data to find coarse estimates of the modal coefficients $A(t)$. Define an inner product (dot product) over some space X as

$$\langle a,b \rangle_X \equiv \int_X a(x)b^T(x)dx = \int_X \begin{bmatrix} a_1(x)b_1(x) & a_1(x)b_2(x) & \cdots \\ a_2(x)b_1(x) & a_2(x)b_2(x) & \\ \vdots & & \ddots \end{bmatrix} dx .$$

Let the space X be the "backbone" surface of the target structure. For example, if the structure is a planar sheet of uniform thickness, then the space X is the 2-D reference surface embedded in the sheet at its equilibrium configuration, and $z(x,t)$ represents the deformation normal to the surface at some location x in X. One useful property of mode shapes is that they are orthogonal in the space X (i.e. $\langle \Phi_i, \Phi_j \rangle_X = 0$ for all $i \neq j$).

Consider a subspace $Y \subset X$, which represents a discrete, not necessarily uniform sampling of the space X (see Fig. 2). The subspace Y is the sample space defined by the range measurements, and may be changing in time.

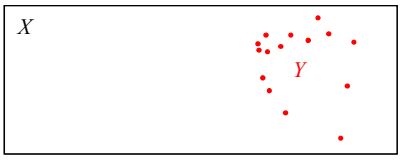

Fig. 2. Sample space Y in complete space X.

In this discrete space the inner product reduces to:

$$\langle a,b \rangle_Y = \sum_{k=1}^{n} a(y_k)b^T(y_k)$$

where y_k is the k^{th} discrete point in the sample space Y and n is the number of discrete points in the sample space.

Define a symmetric modal correlation matrix M_Y to describe the inner products of the mode shapes in the sample space Y, for the m excited modes:

$$M_Y \equiv \langle \Phi, \Phi \rangle_Y = \begin{bmatrix} \langle \Phi_1, \Phi_1 \rangle_Y & \cdots & \langle \Phi_1, \Phi_i \rangle_Y & \cdots & \langle \Phi_1, \Phi_m \rangle_Y \\ \vdots & \ddots & \vdots & \ddots & \vdots \\ \langle \Phi_i, \Phi_1 \rangle_Y & \cdots & \langle \Phi_i, \Phi_i \rangle_Y & \cdots & \langle \Phi_i, \Phi_m \rangle_Y \\ \vdots & \ddots & \vdots & \ddots & \vdots \\ \langle \Phi_m, \Phi_1 \rangle_Y & \cdots & \langle \Phi_m, \Phi_i \rangle_Y & \cdots & \langle \Phi_m, \Phi_m \rangle_Y \end{bmatrix} . \qquad (2)$$

If Y is dense and uniformly distributed over X, then $M_Y \approx \lambda M_X$ for some scale factor λ. However, this paper considers the general case in which the sample space Y is not a uniform and complete sampling of the complete structure space X (e.g. the sensors observe only a portion of the structure). If the sample space is changing (e.g. the sensors are moving), the modal correlation matrix M_Y and the inner product operator $\langle a,b \rangle_Y$ are not constant and must be recomputed using (2) at each time step.

By the Cauchy-Schwarz inequality, it can be shown that M_Y is positive semidefinite [13]. The semidefinite condition arises only from a pathological choice of the sample space Y such that certain modes are unobservable or undiscernable (i.e. the modes are aliased spatially). The condition number (maximum ratio of eigenvalues) of M_Y can be checked to determine the proximity to this condition. All further discussion assumes that M_Y is positive definite, well-conditioned, and invertible.

The sensor measurements are written as

$$\begin{Bmatrix} \bar{z}(y_1,t) \\ \vdots \\ \bar{z}(y_k,t) \\ \vdots \\ \bar{z}(y_n,t) \end{Bmatrix} = \begin{Bmatrix} z(y_1,t) \\ \vdots \\ z(y_k,t) \\ \vdots \\ z(y_n,t) \end{Bmatrix} + \begin{Bmatrix} e_1 \\ \vdots \\ e_k \\ \vdots \\ e_n \end{Bmatrix} \quad \Leftrightarrow \quad \bar{z} = z + e$$

where the overbar is used to denote a measurement, $z(y_k,t)$ is the true deformation of the target at location y_k, and e_k is additive sensor noise.

The modal coefficients $A(t)$ can be recovered through an inner product of the mode shapes with the true deformation of the target:

$$\langle \Phi, z \rangle_Y \equiv \begin{Bmatrix} \langle \Phi_1, z \rangle_Y \\ \vdots \\ \langle \Phi_i, z \rangle_Y \\ \vdots \\ \langle \Phi_m, z \rangle_Y \end{Bmatrix} = M_Y A(t) \quad \Rightarrow \quad A(t) = M_Y{}^{-1} \langle \Phi, z \rangle_Y .$$

Substituting noisy measurements into this equation,

$$\begin{aligned} \breve{A}(t) &= M_Y{}^{-1} \langle \Phi, \bar{z} \rangle_Y \\ &= A(t) + M_Y{}^{-1} \langle \Phi, e \rangle_Y = A(t) + w \end{aligned} \tag{3}$$

where $w \equiv M_Y{}^{-1} \langle \Phi, e \rangle_Y$. By the central limit theorem w is a Gaussian random variable since the number of points in the range image is large. Since it was assumed that noise e is white and unbiased, $E[w] = 0$ and thus (3) is an unbiased estimator of $A(t)$.

The covariance on the coarse estimate $\breve{A}(t)$ is given by

$$\Lambda_{ww} \equiv E[w \cdot w^T] = M_Y{}^{-1} E[\langle \Phi, e \rangle_Y \langle e, \Phi \rangle_Y] M_Y{}^{-1} \tag{4a}$$

If the variance on the noise e is approximately the same for all range image points, this reduces to

$$\Lambda_{ww} = \sigma_e{}^2 M_Y{}^{-1} \tag{4b}$$

where $\sigma_e{}^2 \equiv E[e_k{}^2]$. If the noise variance is substantially different for each range image point, the equations are not as concise but Λ_{ww} is still easily solved [13].

Eq. (3) represents an easily computed coarse estimate of $A(t)$ that is unbiased and has a Gaussian error distribution with statistics computed from (4). It is a minimum-least-square-error estimate of $A(t)$ using data from a single sample time.

IV. Kalman Filtering: Sinusoid Estimation

A Kalman filter is used to observe the time series $\breve{A}(t)$ and extract a better estimate of $A(t)$ using knowledge that it is a weakly decaying sinusoid. Observation over time also allows the estimation of modal parameters.

The estimated state consists of $\hat{A}(t)$, its time rate of change $\hat{V}(t)$, the natural frequencies $\hat{\omega}$, and the modal damping rate $\hat{\alpha}$. If the true modal coefficients follow a decaying sine wave (of arbitrary phase φ_i), their trajectory is given by

$$A_i(t) = \exp(-t\alpha_i)\sin(t\omega_i + \varphi_i).$$

Differentiation and substitution leads to the discrete-time process model

$$\begin{Bmatrix} A_i \\ V_i \\ \omega_i \\ \alpha_i \end{Bmatrix}_{(t+\Delta)} = \begin{Bmatrix} \exp(-\Delta\alpha_i)\cdot\left(A_i \cos(\Delta\omega_i) + \frac{(V_i + \alpha_i A_i)}{\omega_i} \sin(\Delta\omega_i) \right) \\ \exp(-\Delta\alpha_i)\cdot\left(V_i \cos(\Delta\omega_i) - \frac{\alpha_i V_i + (\omega_i{}^2 + \alpha_i{}^2) A_i}{\omega_i} \sin(\Delta\omega_i) \right) \\ \omega_i \\ \alpha_i \end{Bmatrix}_{(t)} + v_i \tag{5}$$

Note the lack of dependence on phase φ_i. If known external forces are applied to the structure (e.g. from robotic systems), then they should be incorporated into the process model here.

Process noise is indicated by $v \equiv \{v_A \quad v_V \quad v_\omega \quad v_\alpha\}^T$, and is characterized by the covariance matrix

$$\Lambda_{vv} \equiv E[vv^T] . \tag{6}$$

The values in this matrix should be chosen to describe the uncertainty in the dynamic model due to unmodeled disturbances and parameter uncertainty.

The Kalman filter measurement model is given by (3). Measurement noise w is white, unbiased, and Gaussian with statistics computed from (4).

The initial a posteriori state estimate is given by

$$\{\hat{A}(0) \quad \hat{V}(0) \quad \hat{\omega}(0) \quad \hat{\alpha}(0)\}^T = \{\breve{A}(0) \quad 0 \quad \hat{\omega}_{exp} \quad \hat{\alpha}_{exp}\}^T \tag{7}$$

where ω_{exp} and α_{exp} are the expected frequencies and damping predicted offline beforehand. For lack of better information, the estimated time rate of change of $A(t)$ is initialized to the unbiased value zero.

The initial a posteriori state error covariance should be chosen to describe the uncertainty in (7). The covariance on $\hat{A}(0)$ will be the measurement covariance given by (4) while the other portions of the state covariance must be based engineering judgment of the actual system.

The implementation of the Kalman filter is straightforward using (3-7). Since the process model is nonlinear, an extended Kalman filter, unscented Kalman filter, particle filter, or a more general form of Bayesian filter must be used. The unscented Kalman filter [14] was used here with very good observed performance.

V. Shape Estimation: Modal Reconstruction

Shape estimation is simply a modal reconstruction using (1) and the estimated modal coefficients:

$$\hat{z}(x,t) = \sum_{i=1}^{m} \hat{A}_i(t)\hat{\Phi}_i(x) = \hat{A}(t)^T \hat{\Phi}(x). \tag{8}$$

The hat notation is used on the mode shapes $\Phi(x)$ as a reminder that the estimator might not know these perfectly, as they are based on theoretical analyses performed offline.

If mode shape knowledge is perfect, the uncertainty in the shape estimate is given by

$$\begin{aligned} \Lambda_{zz}(x,t) &\equiv E[(\hat{z}(x,t) - z(x,t))(\hat{z}(x,t) - z(x,t))^T] \\ &= \Phi(x)^T \Lambda_{\hat{A}\hat{A}}(t) \Phi(x) \end{aligned} \tag{9}$$

where $\Lambda_{\hat{A}\hat{A}}(t)$ is the error covariance on the estimate $\hat{A}(t)$. Analysis suggests that mode shape uncertainty degrades estimator performance gracefully rather than catastrophically [13], however a full discussion of this topic is beyond the scope of this paper.

VI. Results

A. Simulation Studies

Computer simulations were used to study estimator performance. Representative space structures were built into a virtual environment created with OpenGL. Structural models used here are representative of state-of-the-art deployable space structures [1]. Fig. 3 shows a simulated structure that is representative in scale and stiffness of proposed space solar power systems [4][5]. Each triangular element has a 200-meter side length, yielding a structure approximately 2 km by 2 km in size. The first mode of vibration has a period of approximately 40 minutes and the one-hundredth mode has a period of approximately 40 seconds [1]. The modes were energy-normalized so that a modal coefficient of 1.0 indicated the same elastic potential energy for all modes. The simulated structure was given a random excitation on the interval $0 \le A_{i\max} \le 1$, making the expected energy the same for all modes. Phase for each mode was randomly selected over the interval $0 \le \varphi_i < 2\pi$. For initial studies, damping was zero, all the active modes were estimated, and the mode shapes were known perfectly by the estimator.

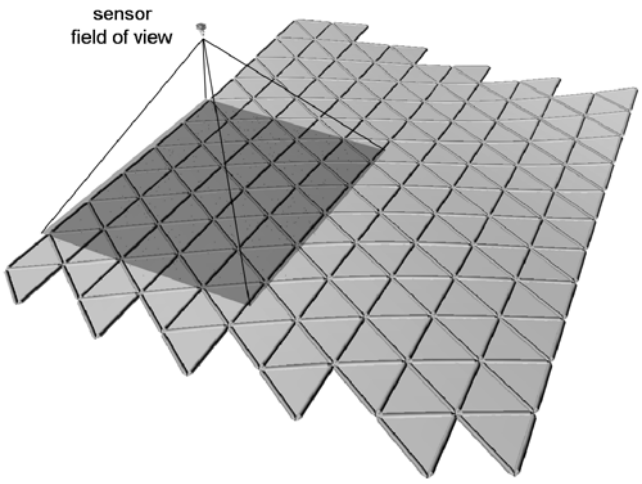

Fig. 3. Planar space structure used in simulation studies. Vibrations occur out-of-plane. Simulated range imager and its field of view are shown.

A single simulated sensor was placed in this environment and its range images were synthesized. The sensor has a resolution of 30 by 30 pixels and a field of view of 80 degrees. The sensor was placed so that it observed approximately one-quarter of the structure (see Fig. 3). Range images were taken at a rate of one per simulated minute. Gaussian noise was added to the synthetic range images, with a standard deviation of 3% of the measurement in the range direction. This value is similar to that found in practical sensors proposed for space applications [10][11].

Fig. 4 shows typical simulation results for the surrogate measurements $\breve{A}(t)$ and filtered estimates $\hat{A}(t)$ of a few modal coefficients. These results are similar for all modes, regardless of number estimated, as long as the Nyquist sampling criterion is met with respect to the modal frequencies. Note that the signal-to-noise ratio is different for each mode, which is due to the sample space chosen, which affects the matrix M_Y and therefore the noise on the surrogate measurement (see (5b)).

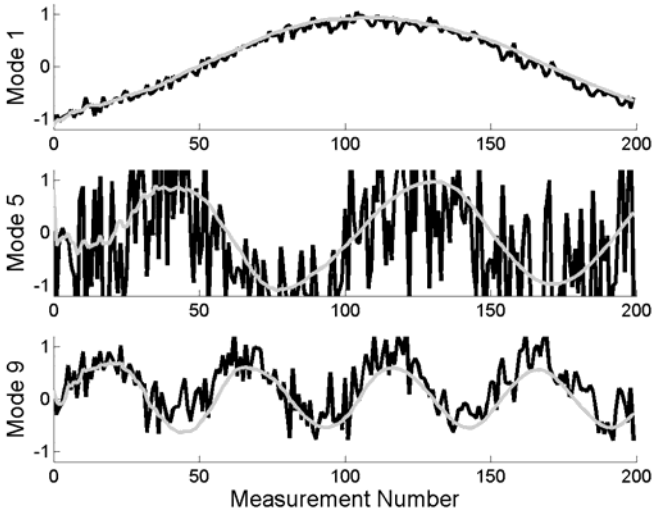

Fig. 4. Surrogate measurements of modal coefficients (black lines), with results of Kalman filtering superimposed (gray lines) (simulation results).

Fig. 5 shows frequency estimation histories for these simulations. Again, these results are typical for any number of modes estimated, as long as the Nyquist sampling criterion is met for each mode. Note that all frequencies are correctly estimated within a few periods of vibration.

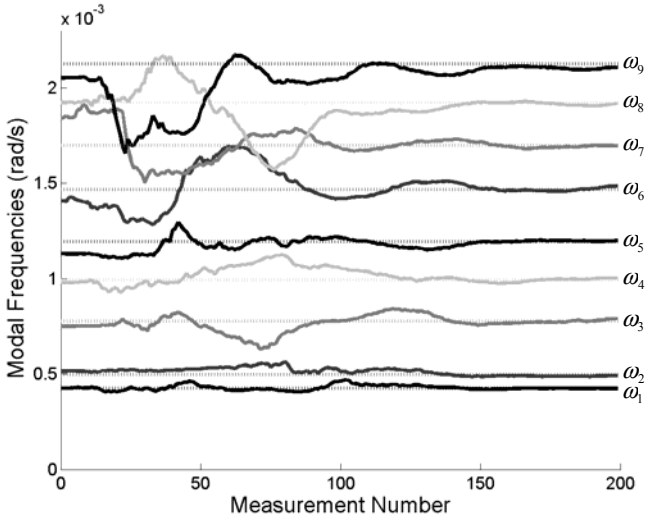

Fig. 5. Frequency estimates (simulation results). Dotted lines indicate true values.

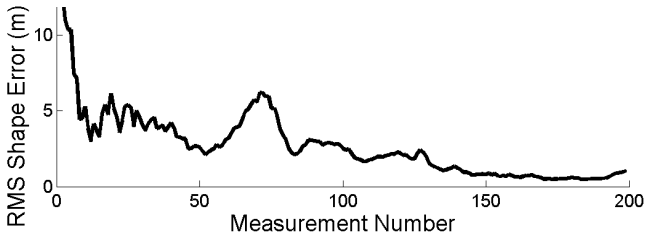

Fig. 6. Shape estimation error vs. time, with all excited modes estimated (simulation results). Amplitude of vibration is approximately 25 m.

Fig. 6 shows overall shape estimation errors as a function of time. Shape estimation error is defined here as the root-mean-square (RMS) estimation error computed

over the entire structure surface. Note that shape is quickly estimated within one or two periods of vibration of the lowest natural frequency. The spike in the estimation error around measurement 70 arises because the process model is nonlinear and many parameter estimates are still converging at that time.

Simulations were used to evaluate the effect of sensor location and field of view on estimator performance. Single and multiple sensors were studied, viewing anywhere from 5% to 100% of the structure, all with similar results to those presented above. The simulations suggest that as long as the modes are observable, estimation is efficient and robust. Increasing sensory noise simply scales up the noise on the coarse estimates $\breve{A}(t)$ (see (4b)), which generally only slows the rate of convergence of the Kalman filter.

B. Experimental Studies

Simple experiments were conducted to assess practical challenges and qualitatively study performance using real hardware. Figs. 7 and 8 show a multi-degree-of-freedom structure used in the experimental studies. It is a quadruple-pendulum composed of four panels and low-friction rotational joints. The upper joint is fixed in inertial space. The experimental model is not instrumented to provide a ground-truth of its motions, and only qualitative results are discussed here.

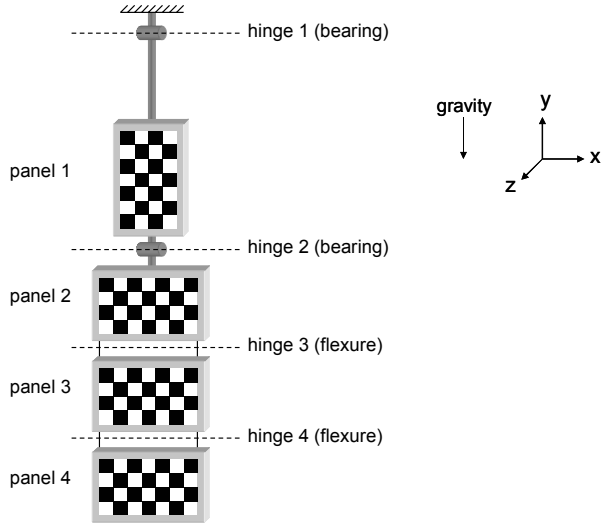

Fig. 7. Multi-degree-of-freedom structure used in experimental studies.

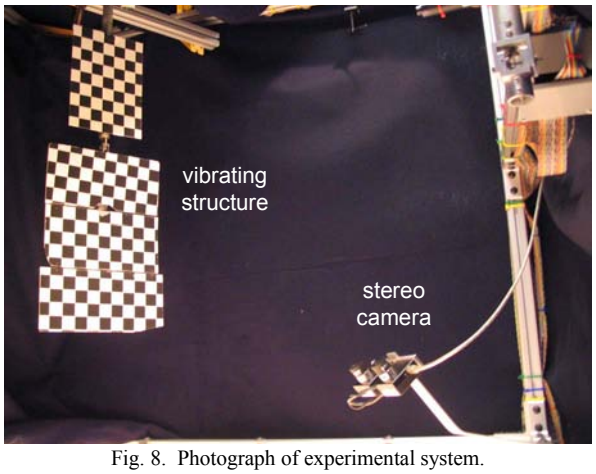

Fig. 8. Photograph of experimental system.

The panels are textured simply to make them visible to stereo cameras, which are used to provide the range images. Note that the textures are *not* used to provide feature sets and specific points are *not* tracked across sample times. The actual pattern is irrelevant to the algorithm, and in practice the natural texture of the target would probably be sufficient for stereo vision systems [12]. Further, the need for texture would be eliminated altogether if a different type of sensor were used (e.g. a laser rangefinder).

Gravity provides a restoring force that causes the structure to vibrate when perturbed. The four dominant modes of vibration involve rotational motions about the four hinges, which are parallel to the x-axis in Fig. 7. Due to backlash in the bearings, several parasitic modes exist that allow limited motions about orthogonal axes (i.e. axes parallel to the y- and z-axes).

The modal frequencies of this structure were empirically derived (to one digit of precision) by timing the actual system with a stopwatch. The approximate mode shapes were provided by digitizing still images of the structure, after exciting each mode of vibration independently. The approximate camera location with respect to the structure was determined manually by visually aligning range images of the structure to geometric models. Certainly, more accurate a priori estimates could be provided; however the intention of using this imprecise method was to explore the estimator's robustness to fairly high a priori uncertainty.

Fig. 9 shows typical experimental results for the surrogate measurements and filtered estimates of the first three modal coefficients. The fourth mode was not estimated since it had very high damping and a frequency near the Nyquist sample rate (the stereo camera used here has a frame rate of 15 Hz).

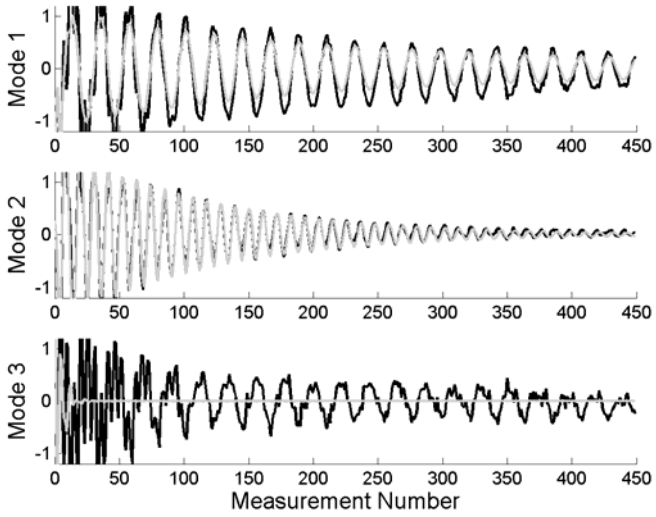

Fig. 9. Modal coefficient surrogate measurements $\breve{A}(t)$ (black) and filtered estimates $\hat{A}(t)$ (gray) vs. time for the first three modes of vibration (experimental results).

Note that the first two modes appear to be estimated accurately, as the filtered results closely follow the measurements in amplitude, phase, frequency, and damping.

It might appear that the third mode is incorrectly estimated at zero. However, closer inspection reveals that the surrogate measurement is dominated by a waveform having the same frequency as that of mode one, not mode three. That is, the mode shapes provided to the estimator were slightly incorrect, and the mode shape error was not orthogonal to the actual first mode shape (i.e. $\left\langle \left(\hat{\Phi}_3 - \Phi_3\right), \Phi_1 \right\rangle_Y \neq 0$). During the determination of the mode shapes, the third mode was observed to damp out in less than two seconds, suggesting that the estimate shown here is correct.

In twenty experimental trials, frequency estimates converged to $\hat{\omega} = \{4.31 \pm 0.01 \quad 8.68 \pm 0.02\}^T$ rad/s and damping estimates converged to $\hat{\alpha} = \{0.049 \pm 0.007 \quad 0.143 \pm 0.008\}^T$ s^{-1} for the first two modes. The third mode typically damped out before the parameters could be estimated. The estimates converged in less than 90 measurements (6 seconds) for all trials. These results seem reasonable considering the fit between estimates and measurements above, and that these are within 10% of the very rough initial estimates provided to the estimator. Visual inspection also revealed good alignment of the range images with the estimated shape.

C. Computation Time

Table 1 shows the estimator computation time required between samples for a 1-GHz Pentium III processor. The empirical relation describing computation time as a function of the number of range points (n) and the number of modes estimated (m) is given approximately by

$$t_{compute} \approx c_1 mn + c_2 m^3$$

where $c_1 \approx 1.4 \times 10^{-6}$ and $c_2 \approx 3.6 \times 10^{-5}$. The cubic term is due to matrix inversions involving matrices of size proportional to m. The bilinear term is due to the inner product computation between range data and each mode shape, which involves summations over a set of size m by n.

TABLE 1. COMPUTATION TIME PER SAMPLE (SECONDS).

		Number of points in range image			
		100	1000	10^4	10^5
Number of modes estimated	10	0.030	0.038	0.18	1.4
	20	0.22	0.24	0.65	4.4
	30	0.87	0.89	1.7	9.1
	40	2.1	2.2	3.5	-
	50	4.6	4.8	6.6	-

Periods of vibration for large space structures can be on the order of tens of minutes. Thus in practice, sensors may only need to sample at a rate on the order of once per minute in order to observe the motions of the structure. Further, it might only be necessary to observe the first ten or twenty modes in order to obtain good shape estimates. Therefore, even with space-qualified hardware, it seems that the computational requirements of the estimator are manageable for real-time implementation.

VII. SUMMARY

This paper has described a methodology for the estimation of modal vibrations using range images. The method exploits a key feature of space applications, which is that the dynamics of objects in space can be modeled accurately. This feature enables an estimator design that is both accurate and robust to the challenging sensing conditions found in space.

A modal decomposition method was developed to handle partial and non-uniform visual sampling of the vibrating target. It was shown that observability of modes is easily checked by computing the condition number of a modal correlation matrix M_Y. Kalman filtering was shown to reduce to a basic sinusoid estimation problem, and shape estimation simply involved modal reconstruction using the estimated modal coefficients.

Simulations and experiments suggested that modal amplitude, phase, frequency, and damping can all be estimated accurately even if the sensors are viewing only a small portion of the structure. Computation time was observed to be very low, suggesting its feasibility for real-time implementation using space-qualified computation.

ACKNOWLEDGMENTS

The authors would like to acknowledge Vickram Mangalgiri for providing detailed structural models for the simulation studies, Dr. Vivek Sujan for fabrication of the experimental testbed, and Dr. Karl Iagnemma, Hiroshi Ueno, Dr. Yoshiaki Ohkami, and Dr. Mitsushige Oda for helpful feedback during the development of this work.

REFERENCES

[1] Mangalgiri, V. "Analysis for the Robotic Assembly of Large Flexible Space Structures." MS Thesis, Dept. of Mech. Eng., MIT, 2004.

[2] Staritz, P.J., S. Skaff, C. Urmson, and W. Whittaker. "Skyworker: A Robot for Assembly, Inspection and Maintenance of Large Scale Orbital Facilities." *Proc. 2001 IEEE Int. Conf. on Robotics and Automation (ICRA 2001)*, Seoul, Korea, pp. 4180-4185, May 2001.

[3] Ueno, H., T. Nishimaki, M. Oda, and N. Inaba. "Autonomous Cooperative Robots for Space Structure Assembly and Maintenance." *Proc. 7th Int. Symp. on Artificial Intelligence, Robotics, and Automation in Space: i-SAIRAS 2003*, NARA, Japan, May 2003.

[4] Mankins, J.C. "A Fresh Look at Space Solar Power: New Architectures, Concepts and Technologies." *Proc. 38th Int. Astronautical Federation Conference*, 1997.

[5] Oda, M., H. Ueno, and M. Mori. "Study of the Solar Power Satellite in NASDA." *Proc. 7th Int. Symp. on Artificial Intelligence, Robotics, and Automation in Space: i-SAIRAS 2003*, NARA, Japan, May 2003.

[6] Maghami, P.G. and S.M. Joshi. "Sensor/Actuator Placement for Flexible Space Structures." *IEEE Trans. on Aerospace and Electronic Systems*, Vol. 29, No. 2, pp. 345-351, April 1993.

[7] Zhang, H.-H. and H.-X. Wu. "Identifiability of Flexible Space Structures." *Proc. IEEE Conf. on Decision and Control*, Vol. 2, pp. 1488-1493, Dec. 1993.

[8] Stieber, M.E., E.M. Petriu, and G. Vukovich. "Systematic Design of Instrumentation Architecture for Control of Mechanical Systems." *IEEE Trans. on Instrument. and Meas.*, Vol. 45, No. 2, pp. 406-412, April 1996.

[9] Scattolini, R. and N. Cattane. "Detection of Sensor Faults in a Large Flexible Structure." *IEE Proc. Control Theory and Applications*, Vol. 146, No. 5, pp. 383-388, Sept. 1999.

[10] Vergauwen, M., M. Pollefeys, and L.J. Van Gool. "A Stereo-vision System for Support of Planetary Surface Exploration." *Machine Vision and Applications*, Vol. 14, No. 1, pp. 5-14, 2003.

[11] Wakabayashi, Y., Y. Ohkami, M. Miyata, T. Adachi, and T. Iijima. "A Compact Laser Range Finder for Space Applications." *Proc. SPIE, Vol. 3714: Enabling Photonic Technologies for Aerospace Applications*, A.R. Pirich, E.W. Taylor, eds., pp. 131-138, 1999.

[12] Jenkin, M. and P. Jasiobedzki. "Computation of Stereo Disparity for Space Materials." *Proc. IEEE Int. Conf. on Intell. Robots and Sys. (IROS)*, 1998.

[13] Lichter, M.D. "Shape, Motion, and Inertial Parameter Estimation of Space Objects using Teams of Cooperative Vision Sensors." PhD Thesis, Dept. of Mech. Eng., MIT, Sept. 2004.

[14] Julier, S.J., and J.K. Uhlmann. "A New Extension of the Kalman Filter to Nonlinear Systems." *Proc. AeroSense: The 11th Int. Symp. on Aerospace/ Defense Sensing, Simulation and Controls*, Orlando, Florida, 1997.